

# Temperature Dependence of In-plane Resistivity and Inverse Hall Angle in NLED Holographic Model

Qingyu Gan, Peng Wang, Haitang Yang

*Center for theoretical physics  
Sichuan University  
Chengdu, 610064, China*

2016222020006@stu.scu.edu.cn, pengw@scu.edu.cn, hyanga@scu.edu.cn

## Abstract

In the strange metal phase of the high- $T_c$  cuprates, it is challenging to explain the linear temperature dependence of the in-plane resistivity and the quadratic temperature dependence of the inverse Hall angle. In this paper, we investigate the temperature dependence of the in-plane resistivity and inverse Hall angle in the nonlinear electrodynamics holographic model developed in our recent work. Maxwell electrodynamics and Born-Infeld electrodynamics are considered. Both cases support a wide spectrum of temperature scalings in parameter space. For Maxwell electrodynamics, the T-linear in-plane resistivity generally dominates at low temperatures and survives into higher temperatures in a narrow strip-like manner. Meanwhile, the T-quadratic inverse Hall angle dominates at high temperatures and extends down to lower temperatures. The overlap between the T-linear in-plane resistivity and the T-quadratic inverse Hall angle, if occurs, would generally present in the intermediate temperature regime. The Born-Infeld case with  $a > 0$  is quite similar to the Maxwell case. For the Born-Infeld case with  $a < 0$ , there can be a constraint on the charge density and magnetic field. Moreover, the overlap can occur for strong charge density.

# 1 Introduction

The holographic techniques developed within string theory [1, 2, 3] have been widely applied in condensed matter physics to explore the properties of strongly correlated systems and undergone some remarkable progress [4, 5, 6, 7, 8, 9, 10, 11, 12].

In present of the strong interactions, the transport properties behave unconventionally in contrast to normal materials which is described by Fermi liquid theorem. A prime example is the strange metal phase emerging from the normal states of the high- $T_c$  cuprates. Among a number of weird transport properties, two of them are celebrated: one is the linear temperature dependence of the in-plane resistivity  $R_{xx}$  and the other is the quadratic temperature dependence of the inverse Hall angle  $\cot \Theta_H$  [13, 14, 15, 16, 17]. A comprehensive review on this aspect could be found in [18]. As early as 90s, some theoretical attempts have been made to explain these behaviors. It is suggested that the scattering of spinons and holons are governed by two different relaxation times in [19], and the independent behaviors of charge conjugation odd and even quasi-particles is proposed in [20].

In recent decade, many holographic models are developed to illustrate and realize these anomalous scalings. The T-linear resistivity is reproduced in [21, 22] by holography. In [23], it claimed that charge-conjugation symmetric conductivity does not contribute to the inverse Hall angle within an Einstein-Maxwell-Dilaton (EMD) model. More EMD-like theories can be found in [24, 25, 26, 27, 28]. In [29], it realized the T-linear resistivity and T-quadratic inverse Hall angle simultaneously in a nonlinear Dirac-Born-Infeld (DBI) model. More DBI-like theories can be found in [30, 31, 32, 33, 34, 35].

Our previous work [36] considered a holographic model with a generic nonlinear electrodynamic (NLED) field. Our NLED holographic model has been taken into account the full backreaction and momentum dissipation following the methods in [34] and [37], respectively. In this paper, We follow up our recent work to investigate the scalings of temperature dependence of  $R_{xx}$  and  $\cot \Theta_H$  in parameter space of this model. Furthermore, we investigate if there is overlap between the T-linear  $R_{xx}$  and T-quadratic  $\cot \Theta_H$ . To extract the effective scalings of temperature, we take advantage of the density plots of  $d \log_{10}(dR_{xx}/dT)/d \log_{10} T$  and  $d \log_{10}(d \cot \Theta_H/dT)/d \log_{10} T$  in parameter space.

The rest of this article is organized as follows. In section 2, we briefly review the holographic model set up in [36] and give the expressions for in-plane resistivity  $R_{xx}$  and inverse Hall angle  $\cot \Theta_H$ . In section 3, we show the density plots of  $d \log_{10}(dR_{xx}/dT)/d \log_{10} T$  and  $d \log_{10}(d \cot \Theta_H/dT)/d \log_{10} T$  in various parameter spaces to study the scalings of temperature dependence of  $R_{xx}$  and  $\cot \Theta_H$ . We focus on two typical cases: one is Maxwell electrodynamics and the other is nonlinear Born-Infeld electrodynamics which are discussed in subsections 3.1 and 3.2, respectively. In section 4, we end in short conclusions and discussions.

## 2 Holographic Setup and DC Conductivity

Consider a holographic model with the action given by

$$S = \int d^4x \sqrt{-g} [R - 2\Lambda - \frac{1}{2} \sum_{I=1}^2 (\partial\psi_I)^2 + \mathcal{L}(s, p)], \quad (2.1)$$

where  $\Lambda = -3/l^2$ , and we take  $16\pi G = 1$  and  $l = 1$  for simplicity. To break translational symmetry and generate momentum dissipation, we introduce two axions  $\psi_I$  ( $I = 1, 2$ ), which lead to a finite DC conductivity [37, 38]. In the action (2.1), the generic NLED Lagrangian  $\mathcal{L}(s, p)$  is a function of  $s$  and  $p$ , where  $s \equiv -F^{ab}F_{ab}/4$  and  $p \equiv -\epsilon^{abcd}F_{ab}F_{cd}/8$  (the indices  $a, b \dots$  denote the bulk spacetime  $t, r, x$  and  $y$ ). The two independent nontrivial scalars  $s$  and  $p$  are built from the electromagnetic field  $A_a$  using field strength tensor  $F_{ab} = \partial_a A_b - \partial_b A_a$  and totally anti-symmetric Lorentz tensor  $\epsilon^{abcd}$ .

Along the lines of [36], we take the following ansatz to construct a black brane solution with asymptotic AdS spacetime:

$$\begin{aligned} ds^2 &= -f(r)dt^2 + \frac{dr^2}{f(r)} + r^2(dx^2 + dy^2), \\ \mathbf{A} &= A_t(r)dt + \frac{h}{2}(xdy - ydx), \\ \psi_1 &= \alpha x, \\ \psi_2 &= \alpha y, \end{aligned} \quad (2.2)$$

where  $h$  denotes the magnetic field and  $\alpha$  denotes the strength of momentum dissipation. Plugging the ansatz into the action (2.1) and varying it with respect to  $g_{ab}$ ,  $A_a$  and  $\psi_I$ , we obtain the equations of motions:

$$f(r) - 3r^2 + rf'(r) = -\frac{\alpha^2}{2} + \frac{r^2}{2}[\mathcal{L}(s, p) + A'_t(r)G^{rt}], \quad (2.3)$$

$$2f'(r) - 6r + rf''(r) = r[\mathcal{L}(s, p) + hG^{xy}], \quad (2.4)$$

$$[r^2G^{rt}]' = 0, \quad (2.5)$$

where the prime denotes the derivative to radial direction, and  $G$  is defined as  $G^{ab} \equiv -\partial\mathcal{L}(s, p)/\partial F_{ab}$ . Eqn. (2.5) leads to  $G^{rt} = -\rho/r^2$ , where  $\rho$  could be interpreted as the charge density of the dual field theory [36]. The horizon located at  $r_h$  is determined by  $f(r_h) = 0$ , and the Hawking temperature is given by  $T = f'(r_h)/4\pi$ . Therefore, eqn. (2.3) gives

$$-3r_h^2 + 4\pi r_h T = -\frac{\alpha^2}{2} + \frac{r_h^2}{2}[\mathcal{L}(s_h, p_h) + A'_t(r_h)G_h^{rt}] \quad (2.6)$$

with

$$\begin{aligned} s_h &= \frac{A_t'^2(r_h)}{2} - \frac{h^2}{2r_h^4}, \\ p_h &= -\frac{hA'_t(r_h)}{r_h^2}, \\ G_h^{rt} &= -\frac{\rho}{r_h^2} = -\mathcal{L}^{(1,0)}(s_h, p_h)A'_t(r_h) + \mathcal{L}^{(0,1)}(s_h, p_h)\frac{h}{r_h^2}, \end{aligned} \quad (2.7)$$

where the superscripts (1, 0) and (0, 1) denote the partial derivative of  $\mathcal{L}(s, p)$  with respect to  $s$  and  $p$ , respectively.

Via gauge/gravity duality, the electromagnetic field  $A_a$  living in the bulk would be dual to a conserved current  $\mathcal{J}^i$  (the indices  $i, j \dots$  denote the co-dimensional boundary spacetime  $t, x$  and  $y$ ) living in the boundary. As a consequence, the DC conductivities for  $\mathcal{J}^i$  can be derived using the method developed in [23, 39]. The detailed calculation was carried out in [36], and here we only display the final expressions for DC conductivities  $\sigma$ :

$$\begin{aligned}\sigma_{xx} &= \frac{\alpha^2 r_h^2 \left[ h^2 + \frac{\alpha^2 r_h^2}{\mathcal{L}^{(1,0)}(s_h, p_h)} + A_t'^2(r_h) r_h^4 \right]}{\left[ h^2 + \frac{\alpha^2 r_h^2}{\mathcal{L}^{(1,0)}(s_h, p_h)} \right]^2 + h^2 A_t'^2(r_h) r_h^4}, \\ \sigma_{xy} &= \frac{h A_t'(r_h) r_h^2 \left[ 2\alpha^2 r_h^2 + \mathcal{L}^{(1,0)}(s_h, p_h) (h^2 + A_t'^2(r_h) r_h^4) \right]}{\left[ h^2 + \frac{\alpha^2 r_h^2}{\mathcal{L}^{(1,0)}(s_h, p_h)} \right]^2 + h^2 A_t'^2(r_h) r_h^4} - \mathcal{L}^{(0,1)}(s_h, p_h).\end{aligned}\quad (2.8)$$

To express DC conductivities in terms of the temperature  $T$ , the charge density  $\rho$ , the magnetic field  $h$ , the strength of momentum dissipation  $\alpha$ , we need to solve eqns. (2.3) and (2.5) for  $r_h$  and  $A_t'(r_h)$  and plug them into eqns. (2.8). The in-plane resistivity  $R_{xx}$  and inverse Hall angle  $\cot \Theta_H$  are defined as

$$R_{xx} = \frac{\sigma_{xx}}{\sigma_{xx}^2 + \sigma_{xy}^2} \quad \text{and} \quad \cot \Theta_H = \frac{\sigma_{xx}}{\sigma_{xy}}. \quad (2.9)$$

Notice that  $R_{xx}$  and  $\cot \Theta_H$  remain invariant under the scaling transformation

$$T \rightarrow \lambda T, \alpha \rightarrow \lambda \alpha, h \rightarrow \lambda^2 h, \rho \rightarrow \lambda^2 \rho \quad (2.10)$$

for some positive constant  $\lambda$ . From now on we will rescale  $T, h, \rho$  and  $\alpha$  to  $T/\alpha, h/\alpha^2, \rho/\alpha^2$  and 1 by taking the scaling factor  $\lambda = 1/\alpha$ .

### 3 Temperature Dependence of $R_{xx}$ and $\cot \Theta_H$

In this section we will discuss the scalings of the temperature dependence of the in-plane resistivity  $R_{xx}$  and inverse Hall angle  $\cot \Theta_H$  in parameter space spanned by  $T/\alpha, h/\alpha^2, \rho/\alpha^2$  and some possible parameters from  $\mathcal{L}(s, p)$ . However, the temperature dependence of  $R_{xx}$  and  $\cot \Theta_H$  is highly nontrivial. To compare with the results from experiments, we can fit  $R_{xx}$  and  $\cot \Theta_H$  with some power of  $T/\alpha$ :

$$\begin{aligned}R_{xx} &\sim A + B (T/\alpha)^n, \\ \cot \Theta_H &\sim C + D (T/\alpha)^m,\end{aligned}\quad (3.11)$$

where the terms  $A, B, C$  and  $D$  can depend on  $h/\alpha^2$  and  $\rho/\alpha^2$ . The effective power factors  $n$  and  $m$  are usually focused in experiments since they mainly govern the temperature dependence of  $R_{xx}$  and  $\cot \Theta_H$ . To extract the effective power factors  $n$  and  $m$  from eqn. (3.11), we display the density plots of  $d \log_{10}(dR_{xx}/dT)/d \log_{10} T$  and  $d \log_{10}(d \cot \Theta_H/dT)/d \log_{10} T$  in the parameter space. For latter convenience, we introduce  $N$  and  $M$  as

$$\frac{d \log_{10}(dR_{xx}/dT)}{d \log_{10} T} \equiv N \implies R_{xx} \sim (T/\alpha)^{N+1}, \quad (3.12)$$

$$\frac{d \log_{10}(d \cot \Theta_H / dT)}{d \log_{10} T} \equiv M \implies \cot \Theta_H \sim (T/\alpha)^{M+1}, \quad (3.13)$$

where  $N = 0$  and  $M = 1$  correspond to the linear temperature dependence of in-plane resistivity  $R_{xx}$  and the quadratic temperature dependence of inverse Hall angle  $\cot \Theta_H$ , respectively. In the following, we focus on Maxwell electrodynamics in subsection 3.1 and Born-Infeld electrodynamics in subsection 3.2.

### 3.1 Maxwell Electrodynamics

The Lagrangian for Maxwell Electrodynamics reads

$$\mathcal{L}(s, p) = s. \quad (3.14)$$

Combining eqns. (2.6), (2.7), (2.8), (2.9) and (3.14), one can obtain

$$R_{xx} = \frac{r_h^2 \alpha^2 (h^2 + \rho^2 + r_h^2 \alpha^2)}{r_h^4 \alpha^4 + 2r_h^2 \alpha^2 \rho^2 + h^2 \rho^2 + \rho^4}, \quad (3.15)$$

$$\cot \Theta_H = \frac{r_h^2 \alpha^2 (h^2 + \rho^2 + r_h^2 \alpha^2)}{h \rho (h^2 + \rho^2 + 2r_h^2 \alpha^2)}, \quad (3.16)$$

with the horizon  $r_h$  satisfying

$$-12r_h^4 + 16\pi T r_h^3 + 2\alpha^2 r_h^2 + h^2 + \rho^2 = 0. \quad (3.17)$$

In this paper we focus on  $h/\alpha^2 \geq 0$  and  $\rho/\alpha^2 \geq 0$ , thus  $R_{xx}$  and  $\cot \Theta_H$  are non-negative in Maxwell electrodynamics. We numerically solve eqn. (3.17) for  $r_h$  and then use eqns. (3.15) and (3.16) to study the scalings of temperature dependence of  $R_{xx}$  and  $\cot \Theta_H$ , respectively.

#### 3.1.1 In-plane Resistivity

We depict the density plots of  $d \log_{10}(dR_{xx}/dT)/d \log_{10} T$  at some fixed values of  $h/\alpha^2$  or  $\rho/\alpha^2$  in Figure 1. The vertical axis is labeled by  $\log_{10}(T/\alpha)$ , and the range of the temperature  $T/\alpha$  varies from 0.01 to 100.

From all figures in Figure 1, we find two common features. First, one finds that  $N \sim -3$  at  $T/\alpha \gtrsim 10$ . Actually, in the high temperature limit  $T/\alpha \gg (h/\alpha^2, \rho/\alpha^2)$ , eqn. (3.17) reduces to  $T \propto r_h$ , which leads to

$$R_{xx} \sim \text{constant} + (h^2 - \rho^2)(\alpha T)^{-2} + \mathcal{O}(T^{-4}). \quad (3.18)$$

More interestingly, we find that the resistivity varies linearly in temperature at  $T/\alpha \lesssim 0.1$ .

The density plots of  $d \log_{10}(dR_{xx}/dT)/d \log_{10} T$  versus  $\rho/\alpha^2$  and  $\log_{10}(T/\alpha)$  at  $h/\alpha^2 = 0, 1$  and 10 are displayed in the upper row of Figure 1. At vanishing magnetic field, as one increases the temperature, the corresponding  $N$  monotonically decreases from 0 to  $-3$  at  $\rho/\alpha^2 \lesssim 1$ . However at  $\rho/\alpha^2 \gtrsim 1$ ,  $N$  first increases from 0 to a maximum value and then decreases to  $-3$ . In the  $h/\alpha^2 = 1$  case, the scalings behavior at  $\rho/\alpha \gtrsim 1$  is similar to that in the previous case while at  $\rho/\alpha \lesssim 1$  new behavior appears. One significant character of this new behavior is the discontinuity between the purple region and the red one as shown in the upper middle panel. The line separating these two regions, we call it ‘‘extremum line’’, is determined by  $dR_{xx}/dT = 0$  and thus the value of  $d \log_{10}(dR_{xx}/dT)/d \log_{10} T$  diverges on this line resulting in the discontinuity. Furthermore,  $dR_{xx}/dT = 0$  on the extremum line implies an extreme value of  $R_{xx}$  locally, indicating a transition between

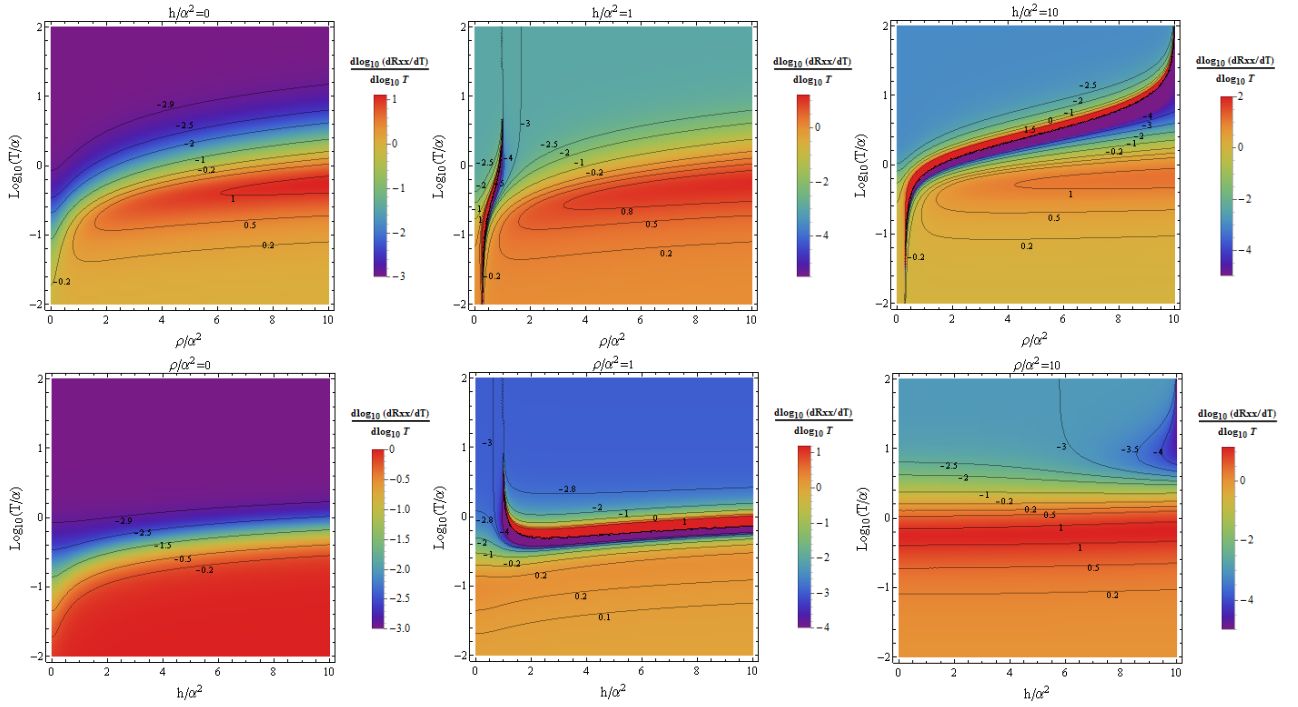


Figure 1: The temperature dependence of  $R_{xx}$  in the Maxwell case. Upper row: Density plots of  $d \log_{10}(dR_{xx}/dT)/d \log_{10} T$  versus  $\rho/\alpha^2$  and  $\log_{10}(T/\alpha)$  at fixed  $h/\alpha^2 = 0, 1$  and  $10$  from left to right. Lower row: Density plots of  $d \log_{10}(dR_{xx}/dT)/d \log_{10} T$  versus  $h/\alpha^2$  and  $\log_{10}(T/\alpha)$  at fixed  $\rho/\alpha^2 = 0, 1,$  and  $10$  from left to right.

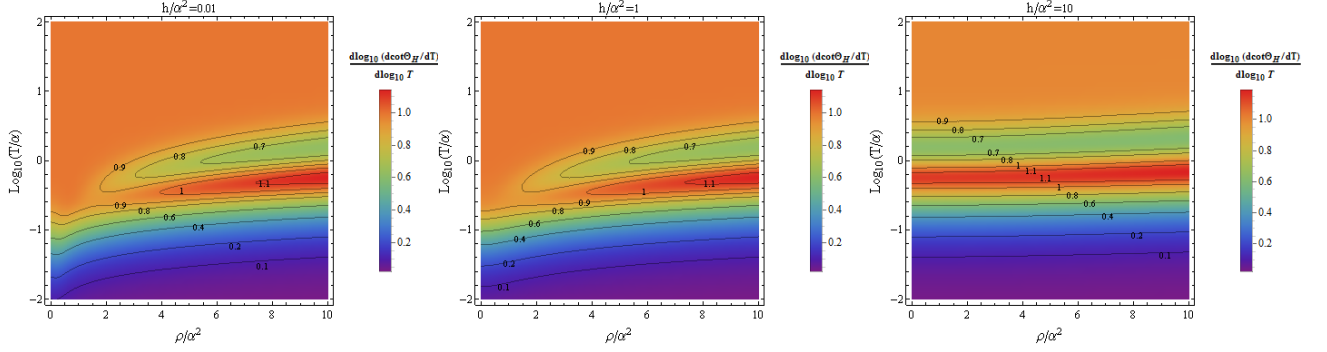


Figure 2: The temperature dependence of  $\cot \Theta_H$  in the Maxwell case. Density plots of  $d \log_{10}(d \cot \Theta_H / dT) / d \log_{10} T$  versus  $\rho / \alpha^2$  and  $\log_{10}(T / \alpha)$  at fixed  $h / \alpha^2 = 0.01, 1$  and  $10$  from left to right.

metal and insulator which is consistent with [36]. The presence of discontinuity provides richer behavior and supports a wider spectrum of temperature scalings. Increasing the magnetic field to  $h / \alpha^2 = 10$ , the extremum line stretches across nearly all the values of  $\rho / \alpha^2$  in the upper right panel. The behavior below the extremum line is similar to the  $h / \alpha^2 = 0$  case, but with much lower scalings exhibits. Due to the discontinuity, a narrow strip-like region of T-linear resistivity survives into  $T / \alpha \gtrsim 1$  above the extremum line.

The density plots of  $d \log_{10}(d R_{xx} / dT) / d \log_{10} T$  versus  $h / \alpha^2$  and  $\log_{10}(T / \alpha)$  at  $\rho / \alpha^2 = 0, 1$  and  $10$  are displayed in the lower row of Figure 1. At vanishing charge density,  $N$  decreases monotonically from about  $0$  to  $-3$  as the temperature increases. In the  $\rho / \alpha^2 = 1$  case, the metal-insulator transition appears and a narrow stripe of T-linear resistivity presents at  $T / \alpha \sim 1$ . For the case with  $\rho / \alpha^2 = 10$ ,  $N$  first increases from  $0$  to  $1$  and then decreases to  $-3$  with the increasing temperature.

To summarize, T-linear resistivity dominates in the low temperature regime with  $T / \alpha \lesssim 0.1$  for almost all the range of  $\rho / \alpha^2$  and  $h / \alpha^2$  in Figure 1 and survives into higher temperatures in a narrow strip-like manner.

### 3.1.2 Inverse Hall Angle

We display the density plots of  $d \log_{10}(d \cot \Theta_H / dT) / d \log_{10} T$  at some fixed values of  $h / \alpha^2$  in Figure 2. Note that  $\cot \Theta_H$  remains invariant under the interchange between  $h / \alpha^2$  and  $\rho / \alpha^2$  from eqns. (3.16) and (3.17). Eqn. (3.16) shows that  $\cot \Theta_H$  diverges at  $h / \alpha^2 = 0$ , so we take a small but non-vanishing magnetic field  $h / \alpha^2 = 0.01$ .

From Figure 2, one can see that  $M \sim 1$  at  $T / \alpha \gtrsim 10$ , indicating the T-quadratic  $\cot \Theta_H$  in the high temperature regime. This is easy to understand from the high temperature limit of eqn. (3.16). At  $T / \alpha \lesssim 0.1$ , we find that  $M \sim 0$ . Similar to  $R_{xx}$ , the inverse Hall angle  $\cot \Theta_H$  behaves linearly in temperature at low temperatures. The two cases with fixed  $\rho / \alpha^2 = 0.01$  and  $\rho / \alpha^2 = 1$  are similar. At  $h / \alpha^2 \gtrsim 4$  the scalings of these two cases both have a non-monotonic behavior. As temperature increases,  $M$  first increases from  $0$  to about  $1$ , then decreases to about  $0.7$ , and then again increases to  $1$ . In the  $h / \alpha^2 = 10$  case, the pattern of the right panel of Figure 2 is similar to those at  $\rho / \alpha^2 \gtrsim 4$  of two previous cases.

To summarize, T-quadratic  $\cot \Theta_H$  not only dominates in the high temperature regime but also extends to much lower temperatures, even reaches  $T / \alpha \sim 0.1$  for small magnetic field and charge density.

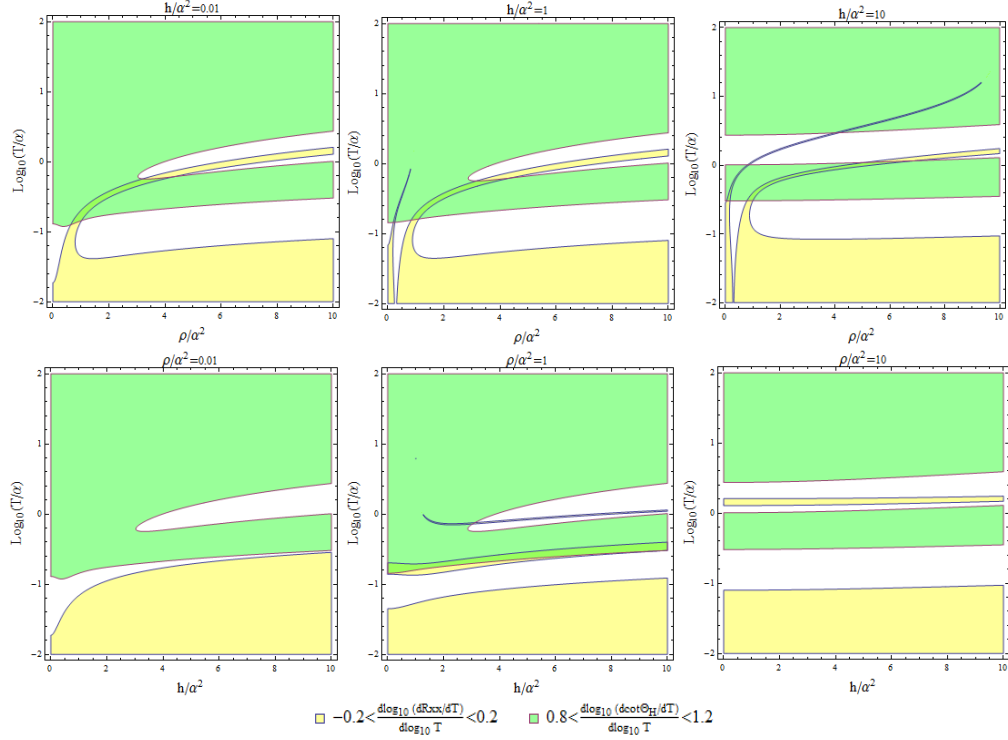


Figure 3: The overlap between T-linear  $R_{xx}$  and T-quadratic  $\cot \Theta_H$  in the Maxwell case. Upper Row: Region plots of  $-0.2 < d \log_{10}(dR_{xx}/dT)/d \log_{10} T < 0.2$  and  $0.8 < d \log_{10}(d \cot \Theta_H/dT)/d \log_{10} T < 1.2$  versus  $\rho/\alpha^2$  and  $\log_{10}(T/\alpha)$  at fixed  $h/\alpha^2 = 0.01, 1$  and  $10$  from left to right. Lower Row: Region plots of  $-0.2 < d \log_{10}(dR_{xx}/dT)/d \log_{10} T < 0.2$  and  $0.8 < d \log_{10}(d \cot \Theta_H/dT)/d \log_{10} T < 1.2$  versus  $h/\alpha^2$  and  $\log_{10}(T/\alpha)$  at fixed  $\rho/\alpha^2 = 0.01, 1$  and  $10$  from left to right. The regions in yellow and green correspond to the T-linear  $R_{xx}$  and the T-quadratic  $\cot \Theta_H$ , respectively.

### 3.1.3 Overlap

We check if there is overlap between the regions of T-linear  $R_{xx}$  and T-quadratic  $\cot \Theta_H$ . We approximately take  $-0.2 < N < 0.2$  as the linear temperature dependence of in-plane resistivity  $R_{xx}$  and  $0.8 < M < 1.2$  as the quadratic temperature dependence of inverse Hall angle  $\cot \Theta_H$ , respectively. In Figure 3, we show the regions of T-linear  $R_{xx}$  and T-quadratic  $\cot \Theta_H$  in yellow and green at some fixed  $h/\alpha^2$  or  $\rho/\alpha^2$ , respectively.

Generally speaking, the T-linear  $R_{xx}$  dominates in the low temperature regime with  $T/\alpha \lesssim 0.1$  and may survive into higher temperatures in a narrow strip-like way, while T-quadratic  $\cot \Theta_H$  dominates in the high temperature regime with  $T/\alpha \gtrsim 10$  and can extend to lower temperatures. The overlap does not occur in the cases with fixed  $\rho/\alpha^2 = 0.01$  and  $10$ . However as shown in Figure 3, there exists the overlap in other cases, which occurs at  $0.1 \lesssim T/\alpha \lesssim 1$ .



## 3.2 Born-Infeld Electrodynamics

Born-Infeld theory is a typical nonlinear realization of electrodynamics arising from the effective string theory at low energy scale with the Lagrange given by

$$\mathcal{L}(s, p) = \frac{1}{a}(1 - \sqrt{1 - 2as - a^2p^2}), \quad (3.19)$$

where the coupling parameter  $a$  is related to the string tension  $\alpha'$  as  $a = (2\pi\alpha')^2$ . To get  $R_{xx}$  and  $\cot \Theta_H$ , we should first obtain  $A'_t(r)$  in terms of  $r_h$ ,  $a$ ,  $h$  and  $\rho$  by eqns. (2.7) and (3.19):

$$A'_t(r_h) = \frac{\rho}{\sqrt{r_h^4 + a(h^2 + \rho^2)}}. \quad (3.20)$$

The reality of  $A'_t(r_h)$  gives a constraint

$$r_h^4 + a(h^2 + \rho^2) > 0. \quad (3.21)$$

For  $a > 0$ , the above constraint holds automatically, while for  $a < 0$  it puts an upper bound on the charge density and magnetic field. The physical interpretation is that the singularity of the black brane needs to hide behind the horizon. After some arrangements of eqns. (2.6), (2.7), (2.8), (2.9), (3.19) and (3.20), the resistivity  $R_{xx}$  and inverse Hall angle  $\cot \Theta_H$  read

$$R_{xx} = \frac{\alpha^2 r_h^2 \left( h^2 + \rho^2 + \alpha^2 \sqrt{r_h^4 + a(h^2 + \rho^2)} \right)}{\alpha^4 r_h^4 + \rho^2 \left( a\alpha^4 + h^2 + \rho^2 + 2\alpha^2 \sqrt{r_h^4 + a(h^2 + \rho^2)} \right)}, \quad (3.22)$$

$$\cot \Theta_H = \frac{\alpha^2 r_h^2 \left( h^2 + \rho^2 + \alpha^2 \sqrt{r_h^4 + a(h^2 + \rho^2)} \right)}{h\rho \left( a\alpha^4 + h^2 + \rho^2 + 2\alpha^2 \sqrt{r_h^4 + a(h^2 + \rho^2)} \right)}, \quad (3.23)$$

with  $r_h$  satisfying

$$-(1 + 6a)r_h^2 + 8\pi a T r_h + a\alpha^2 + \sqrt{r_h^4 + a(h^2 + \rho^2)} = 0. \quad (3.24)$$

For  $|a| \ll 1$ , Maxwell electrodynamics is recovered as expected. Note that  $\cot \Theta_H$  still possesses the symmetry between  $h/\alpha^2$  and  $\rho/\alpha^2$ .

At  $a > 0$ , we find that the temperature dependence of  $R_{xx}$  and  $\cot \Theta_H$  are quite similar to those of Maxwell electrodynamics so we only show some examples in Figure 4. One could find that the behavior in Figure 4 is similar to that in Figures 1 and 2. The slight difference between them is the range of  $N$  and  $M$ . For instance, at  $\rho/\alpha^2 = 0$ , the minimum of  $N$  is  $-3$  in the Maxwell case shown in Figure 1 while it becomes  $-3.5$  in the Born-Infeld case shown in the lower left panel of Figure 4. The similarity among the Maxwell case and Born-Infeld case with  $a > 0$  was also noticed in [34, 36].

Things become quite different in the  $a < 0$  case. In the following, we will discuss the scalings of temperature dependence of  $R_{xx}$  and  $\cot \Theta_H$  in various parameter spaces for  $a < 0$ .

### 3.2.1 In-plane Resistivity

In Figure 5, we depict the density plots of  $d \log_{10}(dR_{xx}/dT)/d \log_{10} T$  at fixed  $a = -1$  and some values of  $h/\alpha^2$  or  $\rho/\alpha^2$ . We would only focus on  $a = -1$  since the cases with other fixed negative value of  $a$  are much alike.

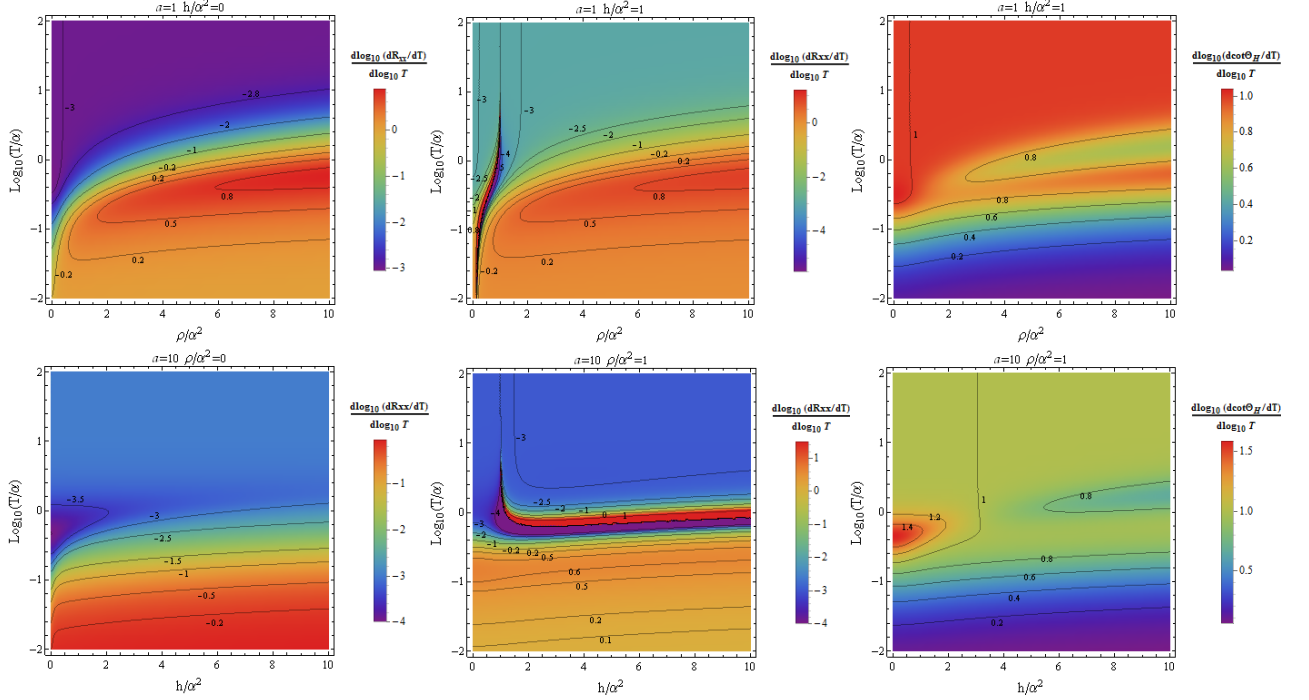


Figure 4: The temperature dependence of  $R_{xx}$  and  $\cot \Theta_H$  in the Born-Infeld case with  $a > 0$ . Density plots of  $d \log_{10}(dR_{xx}/dT)/d \log_{10} T$  and  $d \log_{10}(d \cot \Theta_H/dT)/d \log_{10} T$  for various fixed values of  $a$ ,  $\rho/\alpha^2$  and  $h/\alpha^2$ .

Compared to the case with  $a > 0$ , the most obvious distinction is the appearance of the white region due to the constraint (3.21). The discontinuity usually occurs in the region close to the white region, which implies the metal-insulator transition. The behavior at  $T/\alpha \gtrsim 1$  in Figure 5 is reminiscent of that in Maxwell case. Though the new behavior appears and the range of temperature scalings generally becomes broader for  $a < 0$ , the region of the T-liner resistivity becomes very smaller than that in the  $a > 0$  case.

In the following, we study the temperature dependence of  $R_{xx}$  with respect to the parameter  $a$  since it is a quantity characterizing the coupling of the Born-Infeld electrodynamics. We show the density plots of  $d \log_{10}(dR_{xx}/dT)/d \log_{10} T$  as a function of  $a$  and  $\log_{10}(T/\alpha)$  at various fixed values of  $h/\alpha^2$  and  $\rho/\alpha^2$  in Figure 6. Note that we choose a small but non-vanishing charge density  $\rho/\alpha^2 = 0.01$  in the upper row due to the triviality of constant resistivity  $R_{xx} = 1$  for both strictly vanishing magnetic field and charge density.

We first focus on the upper row with fixed  $\rho/\alpha^2 = 0.01$ . In the  $h/\alpha^2 = 0$  case, there is no white region since  $a$  is not large enough to violate the constraint (3.21). At  $a < 0$ , as the temperature increases,  $N$  first decreases from 0 to  $-\infty$ , then directly jumps to  $+\infty$  on the extremum line and finally decreases to  $-3$  at high temperatures as expected. And at  $a > 0$ , as the temperature increases,  $N$  first decreases from 0 to a minimum around  $-3.5$  and then increases to  $-3$ . The  $h/\alpha^2 = 1$  and  $10$  cases are quite similar to the  $h/\alpha^2 = 0$  case except the appearance of the white region.

We then consider the middle row with fixed  $\rho/\alpha^2 = 1$ . For vanishing magnetic field, at  $a > 0$ ,  $N$  first increases from 0 to a maximum of around 0.5 and then decreases to  $-3$  with the increasing temperature. For the  $h/\alpha^2 = 1$  case,  $N \sim -5$  at sufficiently high temperatures rather than the usual scaling  $-3$ . The reason is

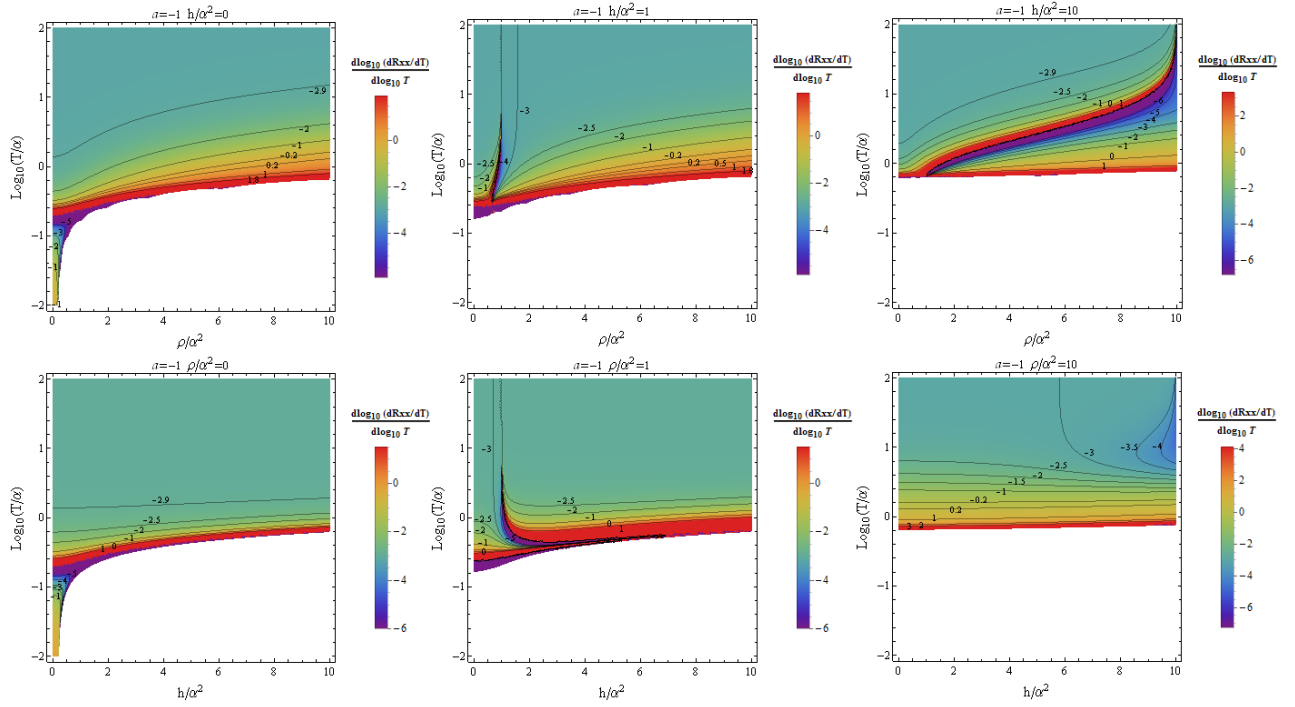


Figure 5: The temperature dependence of  $R_{xx}$  in the Born-Infeld case with  $a = -1$ . Upper Row: Density plots of  $d \log_{10}(dR_{xx}/dT)/d \log_{10} T$  versus  $\rho/\alpha^2$  and  $\log_{10}(T/\alpha)$  at fixed  $h/\alpha^2 = 0, 1$  and  $10$  from left to right. Lower Row: Density plots of  $d \log_{10}(dR_{xx}/dT)/d \log_{10} T$  versus  $h/\alpha^2$  and  $\log_{10}(T/\alpha)$  at fixed  $\rho/\alpha^2 = 0, 1$  and  $10$  from left to right.

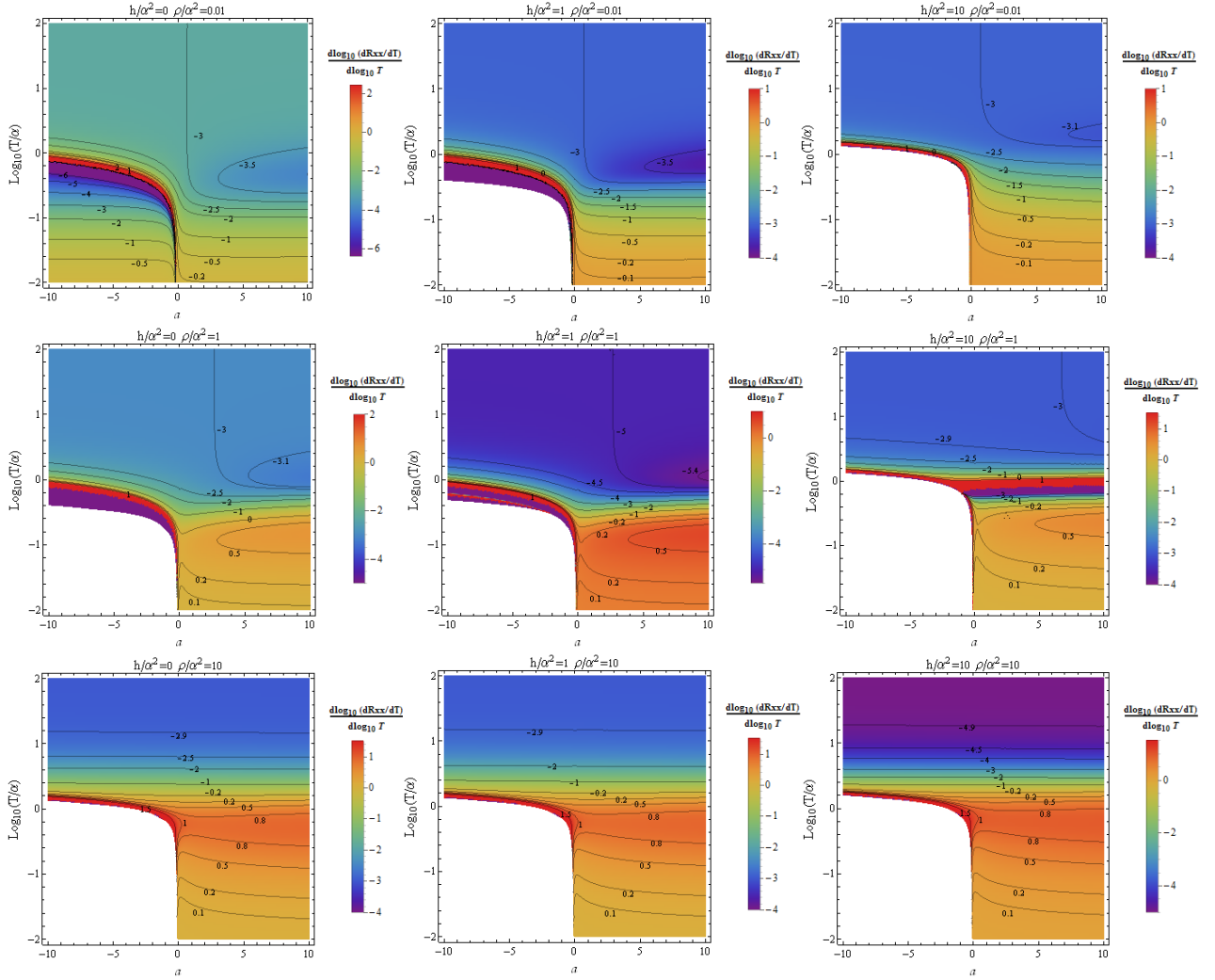


Figure 6: The temperature dependence of  $R_{xx}$  in the Born-Infeld case. Density plots of  $d \log_{10}(dR_{xx}/dT)/d \log_{10} T$  versus  $a$  and  $\log_{10}(T/\alpha)$  at various fixed values of  $h/\alpha^2$  and  $\rho/\alpha^2$ . The fixed  $\rho/\alpha^2$  for each row, from upper to lower, are set as 0.01, 1 and 10. And the fixed  $h/\alpha^2$  for each column, from left to right, are set as 0, 1 and 10.

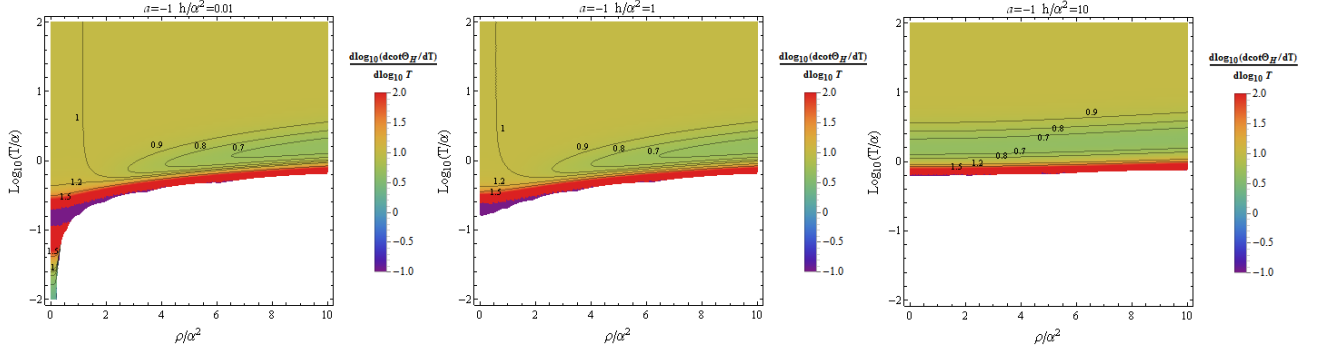


Figure 7: The temperature dependence of  $\cot \Theta_H$  in the Born-Infeld case with  $a = -1$ . Density plots of  $d \log_{10}(d \cot \Theta_H/dT)/d \log_{10} T$  versus  $\rho/\alpha^2$  and  $\log_{10}(T/\alpha)$  at fixed  $h/\alpha^2 = 0.01, 1$  and  $10$  from left to right.

that in high temperature limit, the  $(T/\alpha)^{-2}$  term in eqn. (3.18) vanishes due to  $h/\alpha^2 = \rho/\alpha^2$ , and thus the leading term dependent on the temperature is at the order of  $(T/\alpha)^{-4}$ . Moreover, there are two extremum lines at  $a < 0$ , indicating two metal-insulator transitions at  $T/\alpha \sim 1$ . In the  $h/\alpha^2 = 10$  case, in addition to the expected discontinuity located at  $a < 0$ , a new one appears at  $a > 0$ .

We finally study the the lower row with fixed  $\rho/\alpha^2 = 10$ . In both  $h/\alpha^2 = 0$  and  $h/\alpha^2 = 1$  cases, at  $a > 0$ ,  $N$  first increases from 0 to a maximum of around 1 and then decreases to  $-3$  as the temperature increases. In the case with  $h/\alpha^2 = 10$ , the reason for the unusual scaling at high temperatures is same as that in the case with  $h/\alpha^2 = 1$  and  $\rho/\alpha^2 = 1$ .

Generally speaking, the regions of T-linear  $R_{xx}$  in the Born-Infeld case with  $a > 0$  is similar to those in the Maxwell case. For the Born-Infeld case with  $a < 0$ , they are strips at  $T/\alpha \sim 1$ .

### 3.2.2 Inverse Hall Angle

We now consider the scalings of temperature dependence of the inverse Hall angle. We show the density plots of  $d \log_{10}(d \cot \Theta_H/dT)/d \log_{10} T$  at fixed  $a = -1$  and some values of  $h/\alpha^2$  in Figure 7. The cases at other fixed negative  $a$  are in quite similarity.

The behavior in the upper plane of the three figures in Figure 7 is similar to that in the Maxwell case, which is shown in Figure 2. As before, the white region appears due to the constraint (3.21). The presence of the discontinuity largely widens the spectrum of the temperature scalings of  $\cot \Theta_H$ . Note that a new type discontinuity here could come from the vanishing denominator of  $\cot \Theta_H$  (3.23). Similar to the Maxwell and Born-Infeld with  $a > 0$  cases, the T-quadratic  $\cot \Theta_H$  dominates in the temperature regime with  $T/\alpha \gtrsim 1$ . In the case with  $h/\alpha^2 = 0.01$ , we find that T-quadratic  $\cot \Theta_H$  is observed at low temperatures with  $T/\alpha \sim 0.05$  for weak charge density  $\rho/\alpha^2 \lesssim 0.25$ .

We display the density plots of  $d \log_{10}(d \cot \Theta_H/dT)/d \log_{10} T$  against  $a$  and  $\log_{10}(T/\alpha)$  at various fixed values of  $h/\alpha^2$  and  $\rho/\alpha^2$  in Figure 8. For small but non-vanishing magnetic field and charge density as shown in the upper left panel, no white region exhibits as expected. As the temperature increases,  $M$  increases monotonically from 0.4 to 2 in the region of  $a < 0$  and  $T/\alpha \lesssim 0.1$ . At  $a > 0$ ,  $M$  first increases from 0.2 to a maximum and then decreases to 1. T-quadratic  $\cot \Theta_H$  dominates in  $T/\alpha \gtrsim 1$  for all values of  $a$ , and also

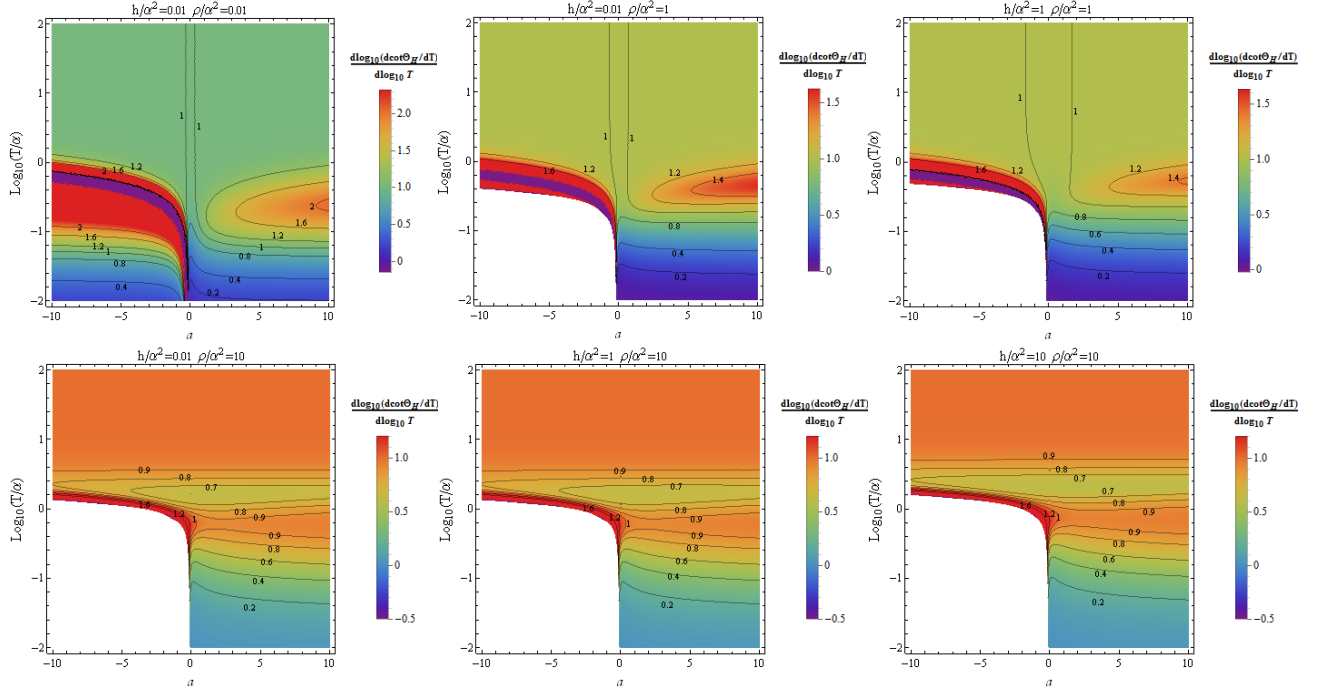


Figure 8: The temperature dependence of  $\cot \Theta_H$  in the Born-Infeld case. Density plots of  $d \log_{10}(d \cot \Theta_H / dT) / d \log_{10} T$  versus  $a$  and  $\log_{10}(T/\alpha)$  at various fixed values of  $h/\alpha^2$  and  $\rho/\alpha^2$  after taking into account the symmetry between  $h/\alpha^2$  and  $\rho/\alpha^2$ .

presents at  $T/\alpha \sim 0.05$  for  $a < 0$ , which is consistent with the  $h/\alpha^2 = 0.01$  case in Figure 7. For the cases in the upper middle and upper right panels, both are similar to the previous case except the presence of the white region. The three cases in lower row are all similar. At  $a > 0$ , with the increasing temperature,  $M$  first increases from 0 to around 0.9, then decreases to around 0.6 and finally increases to 1. The region of T-quadratic  $\cot \Theta_H$  presents in  $T/\alpha \gtrsim 1.5$  and  $0.25 \lesssim T/\alpha \lesssim 1$ .

### 3.2.3 Overlap

We end this section by discussing the overlap between T-linear  $R_{xx}$  and T-quadratic  $\cot \Theta_H$  for Born-Infeld electrodynamics. For the  $a > 0$  case, the overlaps plotted in the  $h/\alpha^2$  ( $\rho/\alpha^2$ )- $\log_{10}(T/\alpha)$  plane with fixed  $a$  are similar to those in the Maxwell cases in Figure 3. For the  $a < 0$  case, the region of T-linear  $R_{xx}$  in the  $h/\alpha^2$  ( $\rho/\alpha^2$ )- $\log_{10}(T/\alpha)$  plane with fixed  $a$  is very small as shown in Figures 5. In Figure 9, we display the region plots of T-linear  $R_{xx}$  in yellow and T-quadratic  $\cot \Theta_H$  in green as a function of  $a$  and  $\log_{10}(T/\alpha)$  at several fixed values of  $h/\alpha^2$  and  $\rho/\alpha^2$ .

Generally speaking, T-linear  $R_{xx}$  mainly lives in low temperatures with  $T/\alpha \lesssim 0.1$  for  $a > 0$  and survives in some strip-like regions at  $T/\alpha \gtrsim 0.1$  for all values of  $a$ . And T-quadratic  $\cot \Theta_H$  dominates at high temperatures for all range of  $a$  and extends down to low temperatures. In the upper row, no overlap exhibits. In the middle row with fixed  $\rho/\alpha^2 = 1$ , the overlap would occur at  $a > 0$  and  $0.1 \lesssim T/\alpha \lesssim 1$ , which is reminiscent of the Maxwell case in Figure 3. In the third row with  $\rho/\alpha^2 = 10$ , a narrow strip-like overlap presents at  $a \lesssim -5$  and  $T/\alpha \sim 1$ , distinguishing from the Maxwell case.

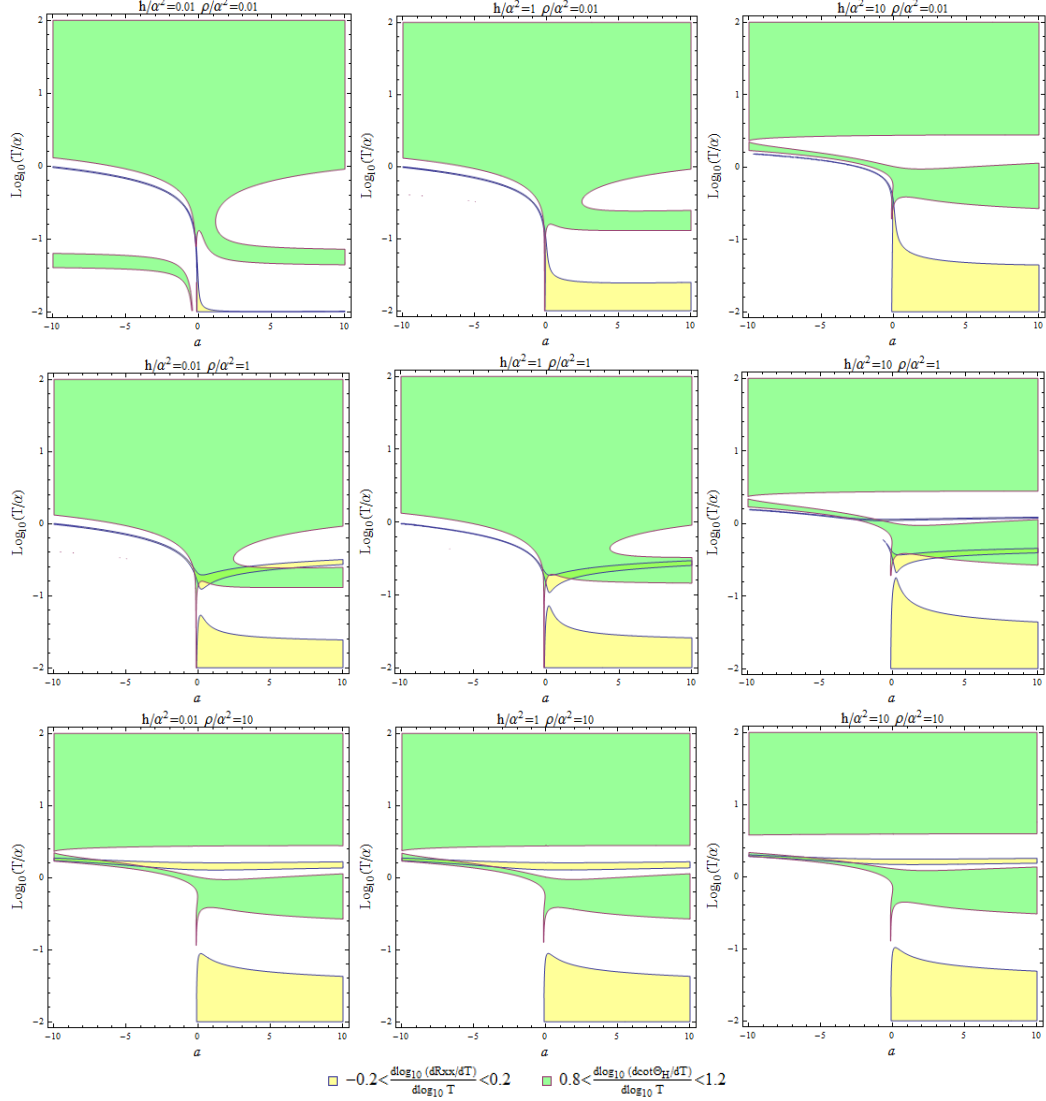


Figure 9: The overlap between T-linear  $R_{xx}$  and T-quadratic  $\cot \Theta_H$  in the Born-Infeld case. Region plots of  $-0.2 < d \log_{10}(dR_{xx}/dT)/d \log_{10} T < 0.2$  and  $0.8 < d \log_{10}(d \cot \Theta_H / dT)/d \log_{10} T < 1.2$  versus  $a$  and  $\log_{10}(T/\alpha)$  for several fixed values of  $h/\alpha^2$  and  $\rho/\alpha^2$ . The fixed  $\rho/\alpha^2$  for each row, from upper to lower, are set as 0.01, 1 and 10. And the fixed  $h/\alpha^2$  for each column, from left to right, are set as 0.01, 1 and 10. The regions in yellow and green correspond to the T-linear  $R_{xx}$  and the T-quadratic  $\cot \Theta_H$ , respectively.

## 4 Discussion and Conclusion

In this paper, we investigated the temperature dependence of the in-plane resistivity  $R_{xx}$  and inverse Hall angle  $\cot \Theta_H$  for the NLED holographic model developed in our previous work [36]. To extract the effective scalings of temperature dependence of  $R_{xx}$  and  $\cot \Theta_H$ , we took the advantage of the density plot of  $d \log_{10}(dR_{xx}/dT)/d \log_{10} T$  and  $d \log_{10}(d \cot \Theta_H/dT)/d \log_{10} T$  in parameter space. In section 3, we focused on two specific cases in the model: one is Maxwell electrodynamics and the other is the nonlinear Born-Infeld electrodynamics.

For Maxwell electrodynamics, a wide spectrum of the scalings of the temperature dependence of  $R_{xx}$  and  $\cot \Theta_H$  can be observed. In general, the in-plane resistivity has been shown to vary as  $R_{xx} \sim T$  at low temperatures and  $R_{xx} \sim T^{-2}$  at high temperatures. And the inverse Hall angle varies as  $\cot \Theta_H \sim T$  at low temperatures and  $\cot \Theta_H \sim T^2$  at high temperatures. Moreover, the presence of discontinuity in the density plot of  $d \log_{10}(dR_{xx}/dT)/d \log_{10} T$  implies the metal-insulator transition. In general, the T-linear  $R_{xx}$  dominates at low temperatures with  $T/\alpha \lesssim 0.1$  and might survives into higher temperatures in a narrow strip-like manner. And the T-quadratic  $\cot \Theta_H$  dominates at high temperatures with  $T/\alpha \gtrsim 10$  and extends down to lower temperatures, even to  $T/\alpha \sim 0.1$  at small magnetic field and charge density. The overlap, if occurs, generally locates in the intermediate temperate regime within  $0.1 \lesssim T/\alpha \lesssim 1$  as shown in Figure 3.

For nonlinear Born-Infeld electrodynamics with  $a > 0$ , the temperature dependence of  $R_{xx}$  and  $\cot \Theta_H$  and their overlap are quite similar to Maxwell case. While at  $a < 0$ , the constraint (3.21) generally results in white region at low temperatures, which provides richer behavior and broader range of scalings than Maxwell case. At  $a < 0$ , the T-linear  $R_{xx}$  presents in a narrow strip-like region at  $T/\alpha \sim 1$  and T-quadratic  $\cot \Theta_H$  still dominates at high temperatures. And the overlap in the  $a < 0$  case could occur at strong charge density as shown in Figure 9.

Notice that we used rescaled quantities, e.g., the rescaled temperature, all the time. However, it is quite unknown how the value of  $\alpha$  is related to experiments. Though the area of the overlap seems small in both electrodynamics, it might explain T-linear  $R_{xx}$  and T-quadratic  $\cot \Theta_H$  simultaneously appearing in experiments for some suitable value of  $\alpha$ . Furthermore, increasing the degrees of freedom in holographic models could enlarge the overlap. For instance, one could introduce the dilaton field which is widely investigated in literatures, e.g., [23, 29, 34].

Finally, we found that in the Maxwell case with vanishing magnetic field, see Figure 1,  $N$  ranges from 0 to 1 at  $T/\alpha \lesssim 1$ . It might imply a combination dependence of temperature  $T + T^2$  on  $R_{xx}$ , which could help to explain the unconventional behaviors observed at low temperatures of two prototypical copper oxide superconductors LSCO and TBCO [40]. It deserves future study to make concrete comparisons with experiments.

### Acknowledgements

We are grateful to Shuxuan Ying and Houwen Wu for useful discussions and valuable comments. This work is supported in part by NSFC (Grant No. 11005016, 11175039 and 11375121).



## References

- [1] T. Banks, W. Fischler, S. H. Shenker and L. Susskind, “M theory as a matrix model: A Conjecture,” *Phys. Rev. D* **55**, 5112 (1997) doi:10.1103/PhysRevD.55.5112 [hep-th/9610043].
- [2] J. M. Maldacena, “The Large N limit of superconformal field theories and supergravity,” *Int. J. Theor. Phys.* **38**, 1113 (1999)[*Adv. Theor. Math. Phys.* **2**, 231 (1998)] doi:10.1023/A:1026654312961 [hep-th/9711200].
- [3] E. Witten, “Anti-de Sitter space and holography,” *Adv. Theor. Math. Phys.* **2**, 253 (1998) doi:10.4310/ATMP.1998.v2.n2.a2 [hep-th/9802150].
- [4] S. S. Gubser, “Breaking an Abelian gauge symmetry near a black hole horizon,” *Phys. Rev. D* **78**, 065034 (2008)doi:10.1103/PhysRevD.78.065034 [arXiv:0801.2977 [hep-th]].
- [5] A. Karch and A. O’Bannon, “Metallic AdS/CFT,” *JHEP* **0709**, 024 (2007) doi:10.1088/1126-6708/2007/09/024 [arXiv:0705.3870 [hep-th]].
- [6] S. A. Hartnoll, C. P. Herzog and G. T. Horowitz, “Building a Holographic Superconductor,” *Phys. Rev. Lett.* **101**, 031601 (2008) doi:10.1103/PhysRevLett.101.031601 [arXiv:0803.3295 [hep-th]].
- [7] S. S. Lee, “A Non-Fermi Liquid from a Charged Black Hole: A Critical Fermi Ball,” *Phys. Rev. D* **79**, 086006 (2009)doi:10.1103/PhysRevD.79.086006 [arXiv:0809.3402 [hep-th]].
- [8] H. Liu, J. McGreevy and D. Vegh, “Non-Fermi liquids from holography,” *Phys. Rev. D* **83**, 065029 (2011) doi:10.1103/PhysRevD.83.065029 [arXiv:0903.2477 [hep-th]].
- [9] M. Cubrovic, J. Zaanen and K. Schalm, “String Theory, Quantum Phase Transitions and the Emergent Fermi-Liquid,” *Science* **325**, 439 (2009)doi:10.1126/science.1174962 [arXiv:0904.1993 [hep-th]].
- [10] S. A. Hartnoll, “Lectures on holographic methods for condensed matter physics,” *Class. Quant. Grav.* **26**, 224002 (2009) doi:10.1088/0264-9381/26/22/224002 [arXiv:0903.3246 [hep-th]].
- [11] C. P. Herzog, “Lectures on Holographic Superfluidity and Superconductivity,” *J. Phys. A* **42**, 343001 (2009) doi:10.1088/1751-8113/42/34/343001 [arXiv:0904.1975 [hep-th]].
- [12] S. A. Hartnoll, A. Lucas and S. Sachdev, “Holographic quantum matter,” arXiv:1612.07324 [hep-th].
- [13] S. Martin, A. T. Fiory, R. M. Fleming, L. F. Schneemeyer and J. V. Waszczak, “Normal state transport properties of  $\text{Bi}_{2+x}\text{Sr}_{2-y}\text{CuO}_6$  crystals,” *Phys. Rev. B* **41**, 846 (1990).
- [14] Y. Ando, S. Komiyama, K. Segawa, S. Ono, and Y. Kurita, “Electronic Phase Diagram of High-Tc Cuprate Superconductors from a Mapping of the In-Plane Resistivity Curvature,” *Phys. Rev. Lett.* **93**, 267001 (2004).
- [15] R. A. Cooper et al. “Anomalous Criticality in the Electrical Resistivity of  $\text{La}_{2x}\text{Sr}_{x-1}\text{CuO}_4$ ,” *Science* **323**,603 (2009).

- [16] T. R. Chien, Z. Z. Wang, and N. P. Ong, “Effect of Zn impurities on the normal-state Hall angle in single-crystal  $YBa_2Cu_{3-x}Zn_xO_{7-\delta}$ ,” *Phys. Rev. Lett.* **67**, 2088 (1991).
- [17] A. W. Tyler and A. P. Mackenzie, “Hall effect of single layer, tetragonal  $Tl_2Ba_2CuO_{6+\delta}$  near optimal doping,” *Physica C* **282-287**, 1185 (1997).
- [18] N. E. Hussey, “Phenomenology of the normal state in-plane transport properties of high-Tc cuprates,” *J. Phys.: Condens. Matter* **20**, 123201 (2008). arXiv:0804.2984v1 [cond-mat.supr-con]
- [19] P. W. Anderson, “Hall effect in the two-dimensional Luttinger liquid,” *Phys. Rev. Lett.* **67** 2092 (1991)
- [20] P. Coleman, A. J. Schoeld and A. M. Tsvelik, “How should we interpret the two transport relaxation times in the cuprates?” *J. Phys: Cond. Matt* **8** 9985 (1996) arXiv:cond-mat/9609009
- [21] S. A. Hartnoll, J. Polchinski, E. Silverstein and D. Tong, “Towards strange metallic holography,” *JHEP* **1004**, 120 (2010) doi:10.1007/JHEP04(2010)120 [arXiv:0912.1061 [hep-th]].
- [22] R. A. Davison, K. Schalm and J. Zaanen, “Holographic duality and the resistivity of strange metals,” *Phys. Rev. B* **89**, no. 24, 245116 (2014) doi:10.1103/PhysRevB.89.245116 [arXiv:1311.2451 [hep-th]].
- [23] M. Blake and A. Donos, “Quantum Critical Transport and the Hall Angle,” *Phys. Rev. Lett.* **114**, no. 2, 021601 (2015) doi:10.1103/PhysRevLett.114.021601 [arXiv:1406.1659 [hep-th]].
- [24] M. Blake, A. Donos and N. Lohitsiri, “Magnetothermoelectric Response from Holography,” *JHEP* **1508**, 124 (2015) doi:10.1007/JHEP08(2015)124 [arXiv:1502.03789 [hep-th]].
- [25] A. Amoretti and D. Musso, “Magneto-transport from momentum dissipating holography,” *JHEP* **1509**, 094 (2015) doi:10.1007/JHEP09(2015)094 [arXiv:1502.02631 [hep-th]].
- [26] Z. Zhou, J. P. Wu and Y. Ling, “DC and Hall conductivity in holographic massive Einstein-Maxwell-Dilaton gravity,” *JHEP* **1508**, 067 (2015) doi:10.1007/JHEP08(2015)067 [arXiv:1504.00535 [hep-th]].
- [27] X. H. Ge, Y. Tian, S. Y. Wu and S. F. Wu, “Hyperscaling violating black hole solutions and Magnetothermoelectric DC conductivities in holography,” *Phys. Rev. D* **96**, no. 4, 046015 (2017) Erratum: [*Phys. Rev. D* **97**, no. 8, 089901 (2018)] doi:10.1103/PhysRevD.96.046015, 10.1103/PhysRevD.97.089901 [arXiv:1606.05959 [hep-th]].
- [28] S. Cremonini, H. S. Liu, H. Lu and C. N. Pope, “DC Conductivities from Non-Relativistic Scaling Geometries with Momentum Dissipation,” *JHEP* **1704**, 009 (2017) doi:10.1007/JHEP04(2017)009 [arXiv:1608.04394 [hep-th]].
- [29] E. Blaauvelt, S. Cremonini, A. Hoover, L. Li and S. Waskie, “Holographic model for the anomalous scalings of the cuprates,” *Phys. Rev. D* **97**, no. 6, 061901 (2018) doi:10.1103/PhysRevD.97.061901 [arXiv:1710.01326 [hep-th]].
- [30] S. S. Pal, “Model building in AdS/CMT: DC Conductivity and Hall angle,” *Phys. Rev. D* **84**, 126009 (2011) doi:10.1103/PhysRevD.84.126009 [arXiv:1011.3117 [hep-th]].

- [31] B. S. Kim, E. Kiritsis and C. Panagopoulos, “Holographic quantum criticality and strange metal transport,” *New J. Phys.* **14**, 043045 (2012) doi:10.1088/1367-2630/14/4/043045 [arXiv:1012.3464 [cond-mat.str-el]].
- [32] A. Karch, “Conductivities for Hyperscaling Violating Geometries,” *JHEP* **1406**, 140 (2014) doi:10.1007/JHEP06(2014)140 [arXiv:1405.2926 [hep-th]].
- [33] E. Kiritsis and L. Li, “Quantum Criticality and DBI Magneto-resistance,” *J. Phys. A* **50**, no. 11, 115402 (2017) doi:10.1088/1751-8121/aa59c6 [arXiv:1608.02598 [cond-mat.str-el]].
- [34] S. Cremonini, A. Hoover and L. Li, “Backreacted DBI Magnetotransport with Momentum Dissipation,” *JHEP* **1710**, 133 (2017) doi:10.1007/JHEP10(2017)133 [arXiv:1707.01505 [hep-th]].
- [35] X. M. Kuang, J. P. Wu and Z. Zhou, “Holographic transports from Born-Infeld electrodynamics with momentum dissipation,” arXiv:1805.07904 [hep-th].
- [36] P. Wang, H. Wu and H. Yang, “Holographic DC Conductivity for Backreacted Nonlinear Electrodynamics with Momentum Dissipation,” arXiv:1805.07913 [hep-th].
- [37] T. Andrade and B. Withers, “A simple holographic model of momentum relaxation,” *JHEP* **1405**, 101 (2014) doi:10.1007/JHEP05(2014)101 [arXiv:1311.5157 [hep-th]].
- [38] M. Blake, R. A. Davison and S. Sachdev, “Thermal diffusivity and chaos in metals without quasiparticles,” *Phys. Rev. D* **96**, no. 10, 106008 (2017) doi:10.1103/PhysRevD.96.106008 [arXiv:1705.07896 [hep-th]].
- [39] A. Donos and J. P. Gauntlett, “Novel metals and insulators from holography,” *JHEP* **1406**, 007 (2014) doi:10.1007/JHEP06(2014)007 [arXiv:1401.5077 [hep-th]].
- [40] R. A. Cooper, Y. Wang, B. Vignolle, O. J. Lipscombe, S. M. Hayden, Y. Tanabe, T. Adachi, Y. Koike, M. Nohara, H. Takagi, C. Proust, N. E. Hussey, “Anomalous Criticality in the Electrical Resistivity of  $La_{2-x}Sr_xCuO_4$ ” *Science* 30 Jan 2009: Vol. 323, Issue 5914, pp. 603-607 DOI: 10.1126/science.1165015